Optimal Fail-Safe Motion Using Dynamic Brake for Lorentz-actuated AFM

Shingo Ito and Georg Schitter
Christian Doppler Laboratory for Precision Engineering for Automated In-Line Metrology,
Automation and Control Institute (ACIN), TU Wien, Vienna, A-1040 Austria
Email: ito@acin.tuwien.ac.at

***Abstract*—Many high-precision motion systems are positioning their mover close to the sample or target with a risk of collision in a failure. In order to prevent damage, this paper proposes a fail-safe system particularly for systems using flexure-guided Lorentz (voice coil) actuators. In this paper, an atomic force microscope (AFM) is used for demonstration. The flexures are deformed during AFM imaging such that the mover with the probe can be withdrawn from the sample by turning off the actuators in a failure. To realize fast withdrawing motion without a sensor for the protection of the probe and sample, this paper also proposes to use the dynamic braking of the Lorentz actuators. For an ideal braking force for fast settling, an optimal dynamic braking resistance is derived to minimize the 2-norm of the mover motion. Because the resulting optimal resistance is negative, it is implemented by an operational amplifier. The experiments demonstrate that the optimal dynamic braking reduces the settling time of the mover by 86.7 %, and the fail-safe operation is completed only within 54 ms.**

I. Introduction

In many precision motion systems with nanometer resolution, a mover is suspended and actuated with respect to a sample or target. Some examples are data storage devices, such as hard disk drives [1] and optical disk drives [2] having a read/write head positioning with respect to a disk. In atomic force microscopes (AFMs), a sharp probe scans over a sample surface for imaging its nanoscale features [3]. Certain vibration isolation systems use Lorentz actuators (e.g. voice coil actuators) to position an instrument (e.g. an AFM head with the probe [4]) with respect to the sample, for high-quality measurement without the influence of the floor vibrations [5].

In a failure of these motion systems, the mover can clash to the target, due to gravity when the power is lost or due to an external shock such as floor vibrations. For hard disk drives, the recording media may be protected by hard materials such as diamond-like carbon [6]. In the case of an AFM, however, its probe is extremely fragile, and the samples can be soft (e.g. photoresists and biological samples). Moreover, in the case of on-site AFMs and the vibration isolation systems, the floor vibrations can excite their mechanical resonances, significantly fluctuating the mover-sample distance, when feedback control is turned off [4], [5]. Due to these factors, there is a high risk of damage in a failure, and a fail-safe system is desired for the motion systems.

This paper proposes a fail-safe system for AFMs using Lorentz actuators as well as for vibration isolation systems positioning an instrument. Fig. 1 illustrates the proposed principle, using a Lorentz-actuated AFM as an example. The mover with the probe is guided by flexures that are modeled by the stiffness k and the damping coefficient c. During an operation, the flexures are vertically deformed by Δz with the actuation force F such that the probe engages with the sample (Fig. 1(a)). When the actuators are turned off in a failure, F immediately becomes zero, and the flexures pull up the probe, disengaging it from the sample to maintain the safety distance Δz for the protection of the probe and the sample (Fig. 1(b)). Due to the simplicity, this fail-safe system is easy to implement and reliable. However, it has a problem that c is usually way smaller than the critical damping [7]. As a result, the suspension mode resulting from the mover mass m and k is strongly excited when the fail-safe system is triggered. The probe oscillates and approaches the sample over and over again, increasing the risk to clash. To solve the problem, the dynamic braking of the Lorentz actuators is utilized for a fast settling motion without oscillation in this paper.

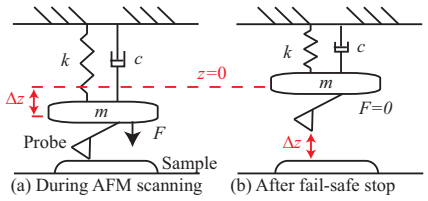

Fig. 1. Principle of fail-safe system. (a) The flexures symbolized by the spring extends Δz during AFM scanning. (b) The mover is lifted by the flexures, disengaging the cantilever form the sample in failure.

Dynamic braking is available by using an electromagnetic actuator as an electrical generator, where the kinetic energy of the mover is dissipated by the resistance of the coil or an additional resistor (i.e. dynamic braking resistor) [8]. The use of dynamic braking force for the fail-safe system may be regarded as an application of active damping with shunt impedance [9]–[11]. Active damping using shunt impedance is typically targeted to suppress externally excited vibrations ideally by maximizing the damping dependent on the configurations [12]–[14]. For the impedance design, active impedance and admittance controllers allow to apply advanced control methods, such as LQR or H_2 control synthesis [12]. However, the resulting controller is typically of high order, and hardware

Post-print version of the article: S. Ito and G. Schitter, "Optimal Fail-Safe Motion Using Dynamic Brake for Lorentz-actuated AFM," *IEEE International Workshop on Advanced Motion Control*, pp. 473-478, 2018. DOI: 10.1109/AMC.2019.8371139

with sufficient power is required for the implementation [12].

In the case of the proposed fail-safe system, the objective is to withdraw the mover from the sample for ensuring a safety distance as quickly as possible, where an adequate braking force, rather than the maximum, is required to suppress the internally excited oscillation (cf. Section V-E). Additionally, for high reliability, it is desired that the hardware implementing the fail-safe system is simple and independent. In order to satisfy these requirements, this paper further investigates the fail-safe system with a dynamic braking resistor and presents methods to determine an optimal resistor value. In the design and implementation for experimental validation, special care is taken to reduce the complexity and the number of components of the fail-safe system, which is desirable to increase the reliability and to decrease the cost.

Section II introduces an AFM system, for which the fail-safe system is experimentally verified without dynamic braking in Section III. To improve the fail-safe motion, the AFM system is modeled in Section IV. An optimal dynamic braking resistance is derived in Section V and implemented in Section VI. Section VII presents the experimental results, and Section VIII concludes the paper.

II. System Description

For experiments, the fail-safe system is implemented for an AFM capable of vibration isolation [15], the block diagram of which is illustrated in Fig. 2. The mover is vertically actuated by two identical flexure-guided Lorentz actuators (AVA2-20, Akribis Systems, Singapore). Since the actuators' Lorentz force is proportional to their coil current I, they are individually driven by a custom-made current amplifier. On the mover, a capacitive displacement sensor (6810(6504-01), MicroSense, Lowell, USA) is installed to measure the distance to the XY stage.

The AFM is intended for the use in vibrational environments, and the floor vibrations fluctuate the position of the probe and the sample. To reject the vibrations, a feedback controller generates the current amplifiers' reference u, based on the displacement sensor signal y_d, such that the distance between the sample and the mover is maintained for AFM imaging. An AFM probe (A-PROBE-10, Nanosensors, Neuchatel, Switzerland) is attached to the mover and outputs the deflection signal y_p. Because the used AFM probe has a relatively large measurement range of about $\pm 200\,\mathrm{nm}$, the deflection signal y_p is directly used to generate an AFM image (i.e. constant height mode [3]).

III. Fail-safe system without dynamic braking

To evaluate the effectiveness of the fail-safe system proposed with Fig. 1, the flexures are deformed downward approximately $20\,\mu\mathrm{m}$, and the feedback controller is turned on to keep the distance between the mover and the sample constant. The safety distance of $20\,\mu\mathrm{m}$ is experimentally determined by measuring the mover response to an impulse-like shock applied to the floor when the feedback controller is turned off. During AFM imaging, the amplifier reference u is set at zero

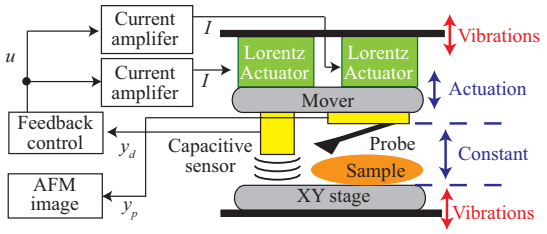

Fig. 2. Block diagram of the AFM capable of vibration isolation [15] used for the implementation of the fail-safe system.

to trigger the fail-safe system while the displacement sensor signal y_d, the AFM deflection signal y_p and u are recorded.

Fig. 3 shows the results, where the fail-safe system is triggered at time $t=0\,\mathrm{s}$. Before $t=0\,\mathrm{s}$, u varies approximately between -50 mA and 100 mA to keep the tip-sample distance constant against the floor vibrations (Fig. 3(c)). As a result, the AFM probe images CD-ROM pits with a height of about 100 nm (Fig. 3(b)). When the fail-safe system is triggered at $t=0\,\mathrm{s}$, Fig. 3(c) shows that u is fixed at zero. The AFM probe disengages from the sample, and y_p immediately gets out of the measurement range in Fig. 3(b). Fig. 3(a) shows that the mover is eventually lifted about $20\,\mu\mathrm{m}$. After this experiment, it is confirmed that the AFM probe is protected and still operational. To check the reliability, this experiment is repeated multiple times. In all the cases, the AFM probe is protected under the vibrational environments, successfully demonstrating the fail-safe system.

Although the experiments validate the effectiveness of the proposed fail-safe system, y_d shows a strong oscillation, and it takes a long time until the mover settles down to ensure the $20\,\mu\mathrm{m}$ safety distance. Particularly at the first swing back, if impulse-like shocks are given to the floor, the probe may break due to a lack of the safety distance. In order to shorten the settling time for the suppression of the swing backs, dynamic braking is utilized in the next sections. As the first step, the AFM system with dynamic braking is modeled.

IV. Modeling

The flexure-guided AFM system can be modeled as a damped mass-spring system, as shown in Fig. 1, where k and c are the stiffness and damping of the flexures, as well as the mover mass m. By using the vertical mover position z and the sum of the Lorentz actuator force F, an equation of motion is given by

$$F = m\frac{\mathrm{d}^2 z}{\mathrm{d}t^2} + c\frac{\mathrm{d}z}{\mathrm{d}t} + kz. \tag{1}$$

When the fail-safe system is triggered at $t=0$, the Lorentz actuators are individually connected to a dynamic braking resistor R_b for the dynamic braking force. In this case, the electric system can be modeled as shown in Fig. 4, resulting in

$$V_{EMF} = (R_b + R)I + L\frac{\mathrm{d}I}{\mathrm{d}t}, \tag{2}$$

Post-print version of the article: S. Ito and G. Schitter, "Optimal Fail-Safe Motion Using Dynamic Brake for Lorentz-actuated AFM," *IEEE International Workshop on Advanced Motion Control*, pp. 473-478, 2018. DOI: 10.1109/AMC.2019.8371139

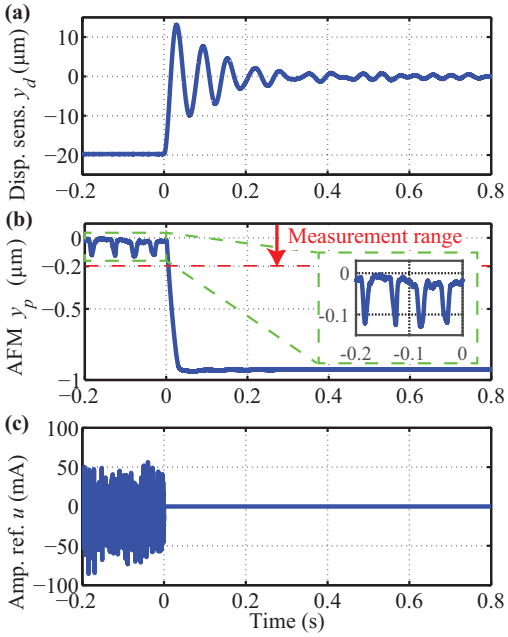

Fig. 3. Recorded signals when the fail-safe system without dynamic braking is triggered at 0 s: (a) displacement sensor signal y_d, (b) AFM deflection signal y_p and (c) amplifier reference u.

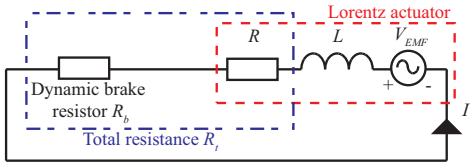

Fig. 4. Electrical model of the AFM system when the fail-safe system is triggered with dynamic braking resistor R_b.

where I and V_{EMF} are the coil current and the back electromotive force (EMF), as well as the resistance R and inductance L of the Lorentz coil. The total Lorentz force F is

$$F = nK_aI, \tag{3}$$

where n and K_a are the number of the Lorentz actuators and their motor constant, respectively. The back EMF is proportional to the velocity of the mover

$$V_{EMF} = -K_e\frac{\mathrm{d}z}{\mathrm{d}t}, \tag{4}$$

where K_e is the back EMF constant. Note that K_a and K_e take the same value in the case of Lorentz actuators [16].

From (1)-(4), a differential equation can be derived as

$$Lm\dddot{z}+(R_tm+Lc)\ddot{z}+(R_tc+Lk+nK_eK_a)\dot{z}+R_tkz=0, \tag{5}$$

where R_t is defined as the total resistance of the electric circuit

$$R_t = R + R_b. \tag{6}$$

The mover position during the fail-safe action can be obtained by solving (5) with the following initial condition at $t=0$

$$z(0)=\Delta z, \quad \left.\frac{\mathrm{d}z}{\mathrm{d}t}\right|_{t=0}=0, \quad \left.\frac{\mathrm{d}^2z}{\mathrm{d}t^2}\right|_{t=0}=0, \tag{7}$$

under an assumption that the mover motion during the AFM imaging is far smaller than the safety distance Δz. The nominal values of the parameters are listed in Table I.

TABLE I
SYSTEM PARAMETERS

Parameter	Value	Unit	Parameter	Value	Unit
m	0.86	kg	R	3.4	Ω
k	13.8	kN/m	K_a	7.20	N/A
c	15.3	N/(m/s)	K_e	7.20	V/(m/s)
L	1.60	mH	n	2	-

V. Optimal Dynamic Braking and Resistor

A. Boundary condition of resistor

The objective of the fail-safe system is to remove all the energy stored in the system in a failure, such that the mover stays at its equilibrium point $z=0$. From the lumped models (Fig. 1 and 4), the total energy $E(t)$ of the system is given by

$$E(t)=\{m\dot{z}^2(t)+kz^2(t)+nLI^2(t)\}/2. \tag{8}$$

The time derivative of the above equation can be arranged by using (1)-(4) with $K_a=K_e$ as follows

$$\dot{E}(t)=-c\dot{z}^2(t)-nR_tI^2(t). \tag{9}$$

To keep removing the energy after triggering the fail-safe system, the above equation needs to be negative for all the time (i.e. $\dot{E}<0$). This requirement gives the lower bound of R_t as follows

$$R_t > -\frac{c\dot{z}^2(t)}{nI^2(t)}, \qquad \text{for} \qquad t>0. \tag{10}$$

The problem of (10) is that the lower bound depends on $\dot{z}(t)$ and $I(t)$, which are the solution of (5). For simplicity, a sufficient condition $R_t > 0$ is used as the lower bound instead. Notice that the above discussion complies with the Lyapunov's stability theorem [17] using $E(t)$ as the Lyapunov function. Thus, with the above sufficient condition, the system is asymptotically stable.

B. Formulation of optimization

Because it can be a measure of the convergence speed of the mover motion, a 2-norm is selected to evaluate a response of the fail-safe system. Additionally, to eliminate the initial condition dependency, the norm is normalized as follows

$$J(R_t)=\frac{||z||_2}{|\Delta z|}=\frac{1}{|\Delta z|}\sqrt{\int_0^\infty z^2(t)\mathrm{d}t}. \tag{11}$$

Using (11) as the objective function, the problem to derive the optimal total resistance $R_{t,opt}$ is formulated for fast withdrawal of the mover as follows

$$R_{t,opt}=\arg\min_{R_t} J(R_t). \tag{12}$$

Post-print version of the article: S. Ito and G. Schitter, "Optimal Fail-Safe Motion Using Dynamic Brake for Lorentz-actuated AFM," *IEEE International Workshop on Advanced Motion Control*, pp. 473-478, 2018. DOI: 10.1109/AMC.2019.8371139

C. Optimal solution

To find the optimal resistance, the objective function $J(R_t)$ needs to be evaluated iteratively. While it is possible to directly compute the solution of the differential equation (5) for a given value of R_t, a method to obtain $J(R_t)$ without solving (5) is desired to reduce the computation time and the numerical errors. In order to do so, Equation (5) with the initial condition (7) is expressed in the form of a state-space model

$$\dot{\mathbf{x}} = \mathbf{A}\mathbf{x}, \tag{13}$$

using the following system matrix $\mathbf{A}$

$$\mathbf{A} = \begin{bmatrix} 0 & 1 & 0 \\ 0 & 0 & 1 \\ -\frac{R_t k}{Lm} & -\left(\frac{R_t c + nK_a K_e}{Lm} + \frac{k}{m}\right) & -\left(\frac{R_t}{L} + \frac{c}{m}\right) \end{bmatrix}, \tag{14}$$

and the state vector $\mathbf{x}$ with its initial condition $\mathbf{x_0}$

$$\mathbf{x} = \begin{bmatrix} z & \dot{z} & \ddot{z} \end{bmatrix}^T, \qquad \mathbf{x_0} = \begin{bmatrix} \Delta z & 0 & 0 \end{bmatrix}^T. \tag{15}$$

The objective function is rewritten with the model as

$$J(R_t) = \frac{1}{|\Delta z|}\sqrt{\int_0^\infty \mathbf{x^T Q x}\mathrm{d}t}, \tag{16}$$

where $\mathbf{Q}$ is a matrix given by

$$\mathbf{Q} = \begin{bmatrix} 1 & 0 & 0 \\ 0 & 0 & 0 \\ 0 & 0 & 0 \end{bmatrix}. \tag{17}$$

Using this matrix, the Lyapunov equation [17] is introduced as follows

$$\mathbf{A^T P} + \mathbf{P A} = -\mathbf{Q}, \tag{18}$$

where $\mathbf{P}$ is a 3×3 matrix. Since the system is stable within $R_t > 0$, Equation (18) can be solved for $\mathbf{P}$, and $J(R_t)$ can be rewritten by replacing $\mathbf{Q}$ in (16) as follows [18]

$$J(R_t) = -\frac{1}{|\Delta z|}\sqrt{\int_0^\infty \frac{\mathrm{d}}{\mathrm{d}t}\left(\mathbf{x^T P x}\right)\mathrm{d}t} = \sqrt{p_{11}}, \tag{19}$$

where p_{11} is the first element in the first column of $\mathbf{P}$.

To obtain p_{11}, (18) is solved by using the MATLAB command *lyap*, and Fig. 5 shows the computed $J(R_t)$ by varying R_t. It can be seen that $J(R_t)$ has the global minimum at $R_t = 1.24\,\Omega$, which is defined as the optimal total resistance $R_{t,opt}$.

D. Analytical solution with $L = 0$

Although the above optimal total resistance required computation, it may be analytically obtained dependent on the system design. Particularly when L is sufficiently small dependent on the Lorentz actuator design, (5) can be approximated by a second-order equation

$$m\ddot{z} + c_t\dot{z} + kz = 0 \tag{20}$$

using the total damping c_t of the mechatronic system [19]

$$c_t = c + nK_eK_a/R_t, \tag{21}$$

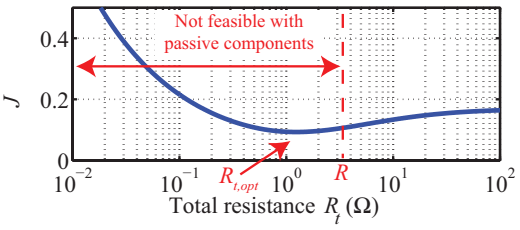

Fig. 5. Computed objective function $J(R_t)$, where $R_{t,opt}$ and R indicate the optimal total resistance and the Lorentz coil resistance, respectively.

which is tunable by R_t. A state-space model of (20) is given with the following state vector and system matrix

$$\mathbf{x} = \begin{bmatrix} z \\ \dot{z} \end{bmatrix}, \ \mathbf{A} = \begin{bmatrix} 0 & 1 \\ -k/m & -c_t/m \end{bmatrix} \text{ for } L = 0. \tag{22}$$

By using the above $\mathbf{A}$ for (18) with

$$\mathbf{Q} = \begin{bmatrix} 1 & 0 \\ 0 & 0 \end{bmatrix}, \tag{23}$$

to derive $\mathbf{P}$, (19) analytically gives the objective function

$$J(R_t) = \sqrt{\frac{c_t^2 + km}{2c_t k}} \qquad \text{for} \qquad L = 0. \tag{24}$$

The derivative of the above function provides the optimal damping $c_t = \sqrt{km}$ that minimizes $J(R_t)$, which corresponds to a damping ratio of 0.5.

The damping ratio of a second-order system is used for design in many applications. In the case of Butterworth filters, the damping ratio is set to 0.70 for the flatness of the pass-band gain [20]. For typical converters, an overshoot of a step response is forbidden, and they are designed to have a damping ratio of one or larger [21]. In comparison with those, the optimal damping of the fail-safe system is smaller, which is beneficial to shorten the rise time of the fail-safe motion. The resulting overshoot is not problematic since the mover goes away from the sample, which justifies the use of the 2-norm in the objective function (11).

From the optimal damping and (21), $R_{t,opt}$ for $L = 0$ is given by

$$R_{t,opt} = nK_eK_a/(\sqrt{km} - c) \qquad \text{for} \qquad L = 0. \tag{25}$$

In the case of the used AFM, the above value is 1.11 Ω, which is 10 % smaller than the computationally obtained value 1.24 Ω. Since this implies that L is too large to ignore for the AFM, $R_{t,opt} = 1.24\,\Omega$ is used for the rest of the paper.

E. Simulation

To analyze the influence of R_t, the position $z(t)$ is simulated for Δz = -20 μm when R_t is set to $10R_{t,opt}$, R, $R_{t,opt}$ and $R_{t,opt}$/10. The simulated results are shown in Fig. 6. With $10R_{t,opt}$, a long lasting oscillation is visible due to a lack of the dynamic braking force. Even if the actuator terminals are shorted for $R_t = R$, the dynamic braking force is insufficient,

Post-print version of the article: S. Ito and G. Schitter, "Optimal Fail-Safe Motion Using Dynamic Brake for Lorentz-actuated AFM," *IEEE International Workshop on Advanced Motion Control*, pp. 473-478, 2018. DOI: 10.1109/AMC.2019.8371139

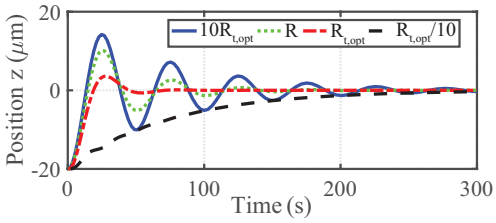

Fig. 6. Simulated position $z(t)$ with the initial value of Δz = -20 μm when R_t takes a value of $10R_{t,opt}$, R, $R_{t,opt}$ and $R_{t,opt}/10$.

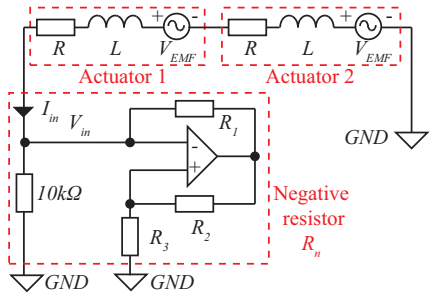

Fig. 7. Circuit of the fail-safe system with a negative resistor.

resulting in swing backs. When $R_{t,opt}/10$ is selected as R_t, the response is slow due to the excessive braking force. In the case of the optimal resistance $R_{t,opt}$, the simulation shows a fast response without an oscillation, demonstrating the effectiveness of the optimal value.

VI. Resistance Implementation

A. Design

When it is smaller than R, R_t cannot be implemented by a passive component as indicated in Fig. 5, because the dynamic braking resistor R_b takes a negative value due to (6). Thus, the optimal resistance $R_{t,opt}$ is realized by an operational amplifier using the circuit in Fig. 7 [22]. To minimize the number of the components, the Lorentz actuators are connected in series with a negative resistor by a relay when the fail-safe system is triggered. The 10 kΩ resistor in the circuit prevents the operational amplifier's input from floating while the Lorentz actuators are disconnected for AFM imaging. Because its value is way larger than the desired total resistance, the 10 kΩ resistor is neglected in the circuit analysis.

By considering the virtual short, the negative resistance R_n of the operational amplifier circuit is given by

$$R_n = V_{in}/I_{in} = -R_1R_3/R_2, \tag{26}$$

where I_{in} and V_{in} are the input current and voltage, respectively. Since most of I_{in} goes through R_1 to the operational amplifier's output, a low cement resistor of 4.7 Ω is selected as R_1 to reduce its thermal dissipation. Since the actuators are connected in series, and $R_{t,opt}$ includes the coil resistance R, R_2 and R_3 are tuned according to (26) to take the following value for the optimal dynamic braking force.

$$R_n = n(R_{t,opt} - r) = -4.32\,\Omega. \tag{27}$$

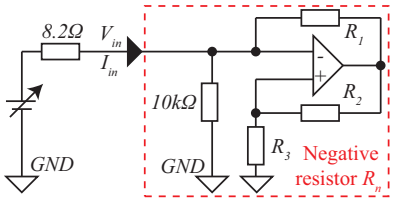

Fig. 8. Test circuit to validate the negative resistor R_n.

B. Validation

For the circuit validation, the relation of the input voltage and current is investigated. The test circuit is shown in Fig. 8. Because a power supply used as the variable voltage source cannot absorb power, R_n is connected with an 8.2 Ω cement resistor in series, such that the total resistance of the test circuit is positive to dissipate power. While the input voltage V_{in} is changed, the input current I_{in} is measured by an oscilloscope (DSO-X 4024A, Keysight, Santa Rosa, USA) with a current probe (1147B, Keysight). From the results, the implemented resistance is determined as -4.48 Ω with a slight implementation mismatch of 3.70 %, which would be due to the tolerance of R_1 ($\pm$ 5%).

VII. Experimental Results

For the experimental validation of the fail-safe system, it is triggered at time t = 0 s while the mover is positioning with feedback control. The measured mover position z in Fig. 9(a) shows a delay of about 10 ms due to the reaction time of the relay. When the Lorentz actuators' terminals are open (i.e. $R_t = \infty$), the position shows a long lasting oscillation without the dynamic braking force. However, by using the implemented negative resistance R_n, a fast response is realized without an oscillation. For a comparison, the settling time with the $\pm$ 5 % band is calculated. When the actuators' terminals are open, the settling time is 406 ms. This long settling time is decreased by 86.7 % to 54.0 ms by implementing the optimal dynamic braking force with the negative resistance.

Fig. 9(b)(c) shows the coil current measured by the current probe (1147B, Keysight) with the nominal noise up to 2.5 $\mathrm{mA_{rms}}$. After the fail-safe system is triggered, the current becomes zero in the case that the actuator terminals are open. When the optimal negative resistance is used in Fig. 9(c), the current shows a peak value of about 10 mA to generate the dynamic braking force. Due to the small current and the short settling time, only a small power is necessary to trigger the fail-safe system (cf. [11]), and a battery or charged capacitor may be used as the power supply, for example in case of a power failure. Overall, the experiments demonstrate that the optimized dynamic braking realizes a fast settling motion

Post-print version of the article: S. Ito and G. Schitter, "Optimal Fail-Safe Motion Using Dynamic Brake for Lorentz-actuated AFM," *IEEE International Workshop on Advanced Motion Control*, pp. 473-478, 2018. DOI: 10.1109/AMC.2019.8371139

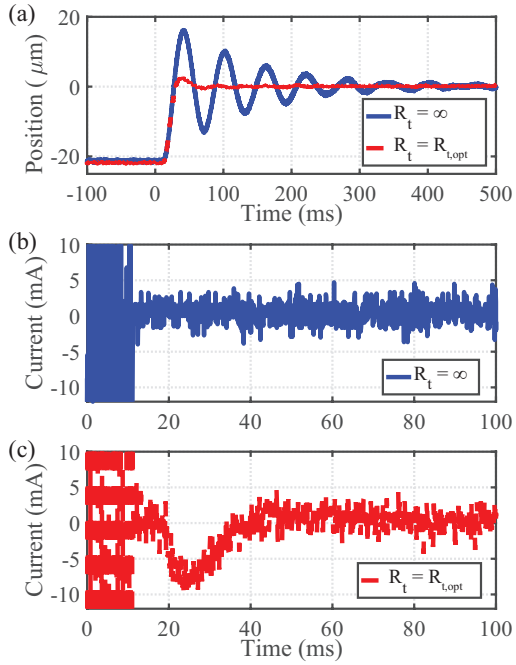

Fig. 9. Measured response with the trigger of the fail-safe system at $t = 0\,\mathrm{s}$ when the actuators' terminals are open (i.e. $R_t = \infty$) and when the optimal total resistance is implemented (i.e. $R_t = R_{t,opt}$): (a) the mover position and (b)(c) the coil current.

withdrawing the mover from the sample for the protection without any sensor as a reliable fail-safe system.

VIII. Conclusion

This paper proposes the fail-safe system that disengages the mover of Lorentz-actuated systems from the sample in case of a failure in a time-optimal way, and an AFM is used for the experiments. While the first experiments demonstrate the protection of the probe attached to the mover, its motion has a long-lasting oscillation, by which the probe approaches the sample over and over again to increase a risk of collision. This problem is solved by introducing the dynamic braking of the Lorentz actuators. For the fast settling of the probe at the safety position, the dynamic braking resistance has been optimized and implemented by means of an operational amplifier for the experiments. The experimental results confirm the effectiveness of the optimal braking force, decreasing the settling time of the mover mounting the probe by 86.7 % without oscillation.

Acknowledgment

This work has been supported in part by the Austrian Research Promotion Agency (FFG) under project number 836489, and in part by the Austrian Federal Ministry of Science, Research and Economy and the National Foundation for Research, Technology and Development, as well as MICRO-EPSILON MESSTECHNIK GmbH & Co. KG and ATENSOR Engineering and Technology Systems GmbH.

References

[1] T. Yamaguchi, M. Hirata, and C. K. Pang, *Advances in High-Performance Motion Control of Mechatronic Systems*. CRC Press, 2013.
[2] A. H. Chaghajerdi, "Sensing and control in optical drives how to read data from a clear disc," *IEEE Control Systems*, vol. 28, no. 3, pp. 23–29, June 2008.
[3] P. Eaton and P. West, *Atomic Force Microscopy*. Oxford University Press, 2010.
[4] S. Ito, S. Unger, and G. Schitter, "Vibration isolator carrying atomic force microscopes head," *Mechatronics*, vol. 44, pp. 32–41, 2017.
[5] R. Saathof, M. Thier, R. Hainisch, and G. Schitter, "Integrated system and control design of a one DoF nano-metrology platform," *Mechatronics*, vol. 47, pp. 88 – 96, 2017.
[6] C. Casiraghi, J. Robertson, and A. C. Ferrari, "Diamond-like carbon for data and beer storage," *Materials Today*, vol. 10, no. 1, pp. 44 – 53, 2007.
[7] S. Ito and G. Schitter, "Comparison and classification of high-precision actuators based on stiffness influencing vibration isolation," *IEEE/ASME Transactions on Mechatronics*, vol. 21, no. 2, pp. 1169–1178, April 2016.
[8] X. Zhou and J. Fang, "Precise braking torque control for attitude control flywheel with small inductance brushless dc motor," *IEEE Transactions on Power Electronics*, vol. 28, no. 11, pp. 5380–5390, Nov 2013.
[9] S. Behrens, A. J. Fleming, and S. O. R. Moheimani, "Passive vibration control via electromagnetic shunt damping," *IEEE/ASME Transactions on Mechatronics*, vol. 10, no. 1, pp. 118–122, Feb 2005.
[10] C. Paulitsch, P. Gardonio, and S. J. Elliott, "Active vibration damping using self-sensing, electrodynamic actuators," *Smart Materials and Structures*, vol. 15, no. 2, p. 499, 2006.
[11] A. Stabile, G. S. Aglietti, G. Richardson, and G. Smet, "Design and verification of a negative resistance electromagnetic shunt damper for spacecraft micro-vibration," *Journal of Sound and Vibration*, vol. 386, no. Supplement C, pp. 38–49, 2017.
[12] A. J. Fleming, S. O. R. Moheimani, and S. Behrens, "Synthesis and implementation of sensor-less active shunt controllers for electromagnetically actuated systems," *IEEE Transactions on Control Systems Technology*, vol. 13, no. 2, pp. 246–261, March 2005.
[13] D. Kohl, D. Mick, T. Riel, R. Saathof, and G. Schitter, "Extending the range of geophones by negative impedance converter," *IFAC-PapersOnLine*, vol. 49, no. 21, pp. 541 – 546, 2016.
[14] S. H. Kamali, M. Moallem, and S. Arzanpour, "Power electronic shunt control for increasing the maximum available damping force in electromagnetic dampers," in *IEEE International Conference on Advanced Intelligent Mechatronics*, July 2017, pp. 1514–1519.
[15] S. Ito and G. Schitter, "Atomic force microscopy capable of vibration isolation with low-stiffness z-axis actuation," *Ultramicroscopy*, vol. 186, pp. 9 – 17, 2018.
[16] R. Munnig Schmidt, G. Schitter, A. Rankers, and J. van Eijk, *The Design of High Performance Mechatronics*, 2nd ed. Delft University Press, 2014.
[17] S. Skogestad and I. Postlethwaite, *Multivariable Feedback Control*. John Wiley, 2005.
[18] H. Kogo and T. Mita, *Introduction to Control System Theory (in Japanese)*. Jikkyo Shuppan Co.,Ltd., 1979.
[19] S. Xie, P. Li, X. Zhang, and B. Yan, "Vibration suppression of structure with electromagnetic shunt damping absorber," *International Journal of Applied Electromagnetics and Mechanics*, vol. 45, pp. 395–402, 2014.
[20] B. Baker, *A Baker's Dozen: Real Analog Solutions for Digital Designers*. Newnes, 2005.
[21] R. W. Erickson and D. Maksimovic, *Fundamentals of Power Electronics*. Springer, 2001.
[22] P. Horowitz and W. Hill, *The Art of Electronics*, 3rd ed. Cambridge University Press, 2015.

Post-print version of the article: S. Ito and G. Schitter, "Optimal Fail-Safe Motion Using Dynamic Brake for Lorentz-actuated AFM," *IEEE International Workshop on Advanced Motion Control*, pp. 473-478, 2018. DOI: 10.1109/AMC.2019.8371139